

Observation of edge solitons and their phase transition in a trimer circuit lattice

Rujiang Li^{1,*}, Xiangyu Kong¹, Wencai Wang¹, Yixi Wang¹,
Yichen Zhong¹, Yongtao Jia¹, Huibin Tao^{2,†}, and Ying Liu^{1‡}

¹*National Key Laboratory of Radar Detection and Sensing,
School of Electronic Engineering, Xidian University, Xi'an 710071, China and*
²*School of Software Engineering, Xi'an Jiaotong University, Xi'an, China*

In nonlinear topological systems, edge solitons emerge either as bifurcations of linear topological edge states or as nonlinearity-induced localized states without topological protection. Although electrical circuits have proven to be a versatile platform for realizing various types of topological insulators, observing edge solitons and their phase transition in circuit lattices remains challenging. Here, we realize quench dynamics in nonlinear electrical circuits and experimentally demonstrate the existence of both topological and nontopological edge solitons in a trimer circuit lattice, as well as the phase transition between these two types of edge solitons. Under weak nonlinearity, we observe antisymmetric and symmetric edge solitons bifurcating from their respective linear topological edge states. In contrast, under strong nonlinearity, nontopological edge solitons with antisymmetric, symmetric, and asymmetric internal structures are discovered. Our work paves the way for exploring exotic nonlinear states and novel phase diagrams in nonlinear topological systems.

Topological insulators are physical structures that act as conventional insulators in the bulk but conduct on their surfaces due to topologically protected edge states [1, 2]. Topological insulators have been realized across diverse physical platforms, and the immunity of topological edge states to local deformations and disorders is crucial for their exciting potential applications [3–11]. Extending topological systems into the nonlinear regime, for instance by considering the nonlinear response of optical materials under high field intensity [12, 13], reveals that the interplay between topology and nonlinearity leads to topological edge solitons, which bifurcate from the linear topological edge states and inherit their topological protection [14–30]. In addition to topological edge solitons, conventional edge solitons, which are nonlinearity-induced localized states at the edge, have also been discovered in nonlinear topological insulators [26–28, 31]. These conventional edge solitons are considered nontopological because they lack a direct connection to the linear topological edge states.

Electrical circuits have recently been proposed as a versatile platform for studying various types of topological insulators [32–36]. Owing to the flexibility in constructing circuit lattices and employing site-resolved, phase-resolved, time-resolved, and frequency-resolved measurement techniques, electrical circuits have proven valuable for exploring high-dimensional [37, 38], higher-order [39, 40], non-Hermitian [41–43], non-Abelian [44, 45], and non-Euclidean topological insulators [46, 47]. Despite some preliminary work on nonlinear topological circuits [48–52], the experimental observation of edge solitons in circuit lattices, particularly the phase transition between topological and nontopological edge solitons, remains challenging.

Here we experimentally implement a nonlinear trimer circuit lattice, which is topological in the linear limit, and observe both topological and nontopological edge solitons

using quench dynamics. We measure the temporal evolutions of site voltages under antisymmetric, symmetric, and single-site excitations, respectively, while tuning the circuit nonlinearity through the excitation voltages. For antisymmetric and symmetric excitations, we consider both weak and strong nonlinearity. Under weak nonlinearity, these excitations create topological edge solitons bifurcating from linear topological edge states. In contrast, under strong nonlinearity, initial voltage distributions lead to nonlinearity-induced conventional edge solitons, indicating a phase transition from topological to nontopological edge solitons. For single-site excitations, we also explore both weak and strong nonlinearity. Under weak nonlinearity, voltage oscillations are observed due to the overlap of antisymmetric and symmetric linear topological edge states. When the excitation voltage exceeds a threshold, voltage localization at a single edge site occurs, forming a nontopological asymmetric edge soliton. Our work offers a general approach to studying solitons in nonlinear circuit lattices, paving the way for exploring exotic nonlinear states and novel phase diagrams in nonlinear topological systems.

We investigate a one-dimensional trimer lattice with onsite nonlinearity, where the onsite energy at each site depends on its corresponding wave function. As shown in Fig. 1a, the nonlinear trimer lattice is described by the following model:

$$i \frac{d\psi_n^A}{dt} = E(\psi_n^A) \psi_n^A + J' \psi_{n-1}^C + J \psi_n^B, \quad (1)$$

$$i \frac{d\psi_n^B}{dt} = E(\psi_n^B) \psi_n^B + J \psi_n^A + J \psi_n^C, \quad (2)$$

$$i \frac{d\psi_n^C}{dt} = E(\psi_n^C) \psi_n^C + J \psi_n^B + J' \psi_{n+1}^A. \quad (3)$$

Here, J and J' represent the intracell and intercell hopping amplitudes, respectively, and $E(\psi_n^{A,B,C})$ denotes the onsite energies which depend on the respective wave

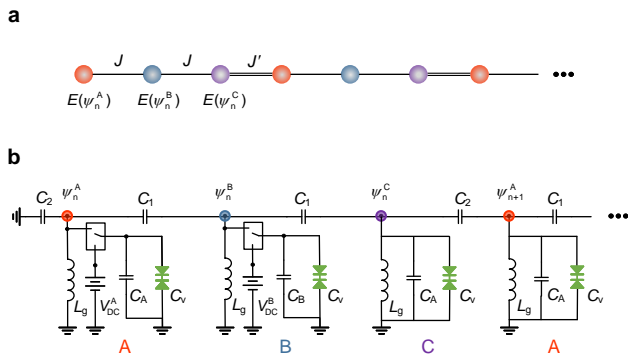


FIG. 1. **a**, Schematic of the nonlinear trimer lattice, where J and J' represent the intracell and intercell hopping amplitudes, respectively, and the onsite energy E at each site depends on the wave function of that site $\psi_n^{A,B,C}$. **b**, Circuit implementation of the nonlinear trimer lattice. The node voltages correspond to the wave functions at the lattice sites. Capacitors C_1 and C_2 emulate the intracell and intercell hopping amplitudes, respectively. The onsite nonlinearity is achieved through common-cathode diodes, which exhibit voltage-dependent capacitance C_v . In the two leftmost nonlinear LC oscillators, SPDT switches and DC voltage sources are employed to implement the quench dynamics.

functions. This model can be implemented using a nonlinear circuit lattice as illustrated in Fig. 1b. Each unit cell comprises three nonlinear LC resonators with an inductor L_g , capacitors C_A or C_B , and common-cathode diodes C_v . The capacitance of the common-cathode diode is expressed as $C_v = \frac{C_L}{(1+|v/v_0|)^M}$, where C_L , v_0 , and M are constants, and v is the voltage amplitude applied across its terminals (see Supplementary Note 1 for the modeling of common-cathode diodes). The nonlinear resonators are coupled via capacitors $C_{1,2}$. In the two leftmost resonators, single-pole double-throw (SPDT) switches control the charging and discharging of capacitors $C_{A,B}$ and diodes C_v .

From Fig. 1b, when the SPDT switches are connected to the DC voltage sources, the capacitors $C_{A,B}$ and diodes C_v are charged to the constant voltages $V_{DC}^{A,B}$. This charging operation corresponds to preparing the initial state, and the phase of this initial state can be adjusted by the DC voltage sources. Once the SPDT switches are simultaneously toggled to the circuit nodes, the charged capacitors and diodes discharge, with the temporal evolution of the initial voltage distribution governed by Eqs. (1)-(3) (see Supplementary Note 1 for circuit equations and implementation of quench dynamics). The voltage envelopes at the circuit nodes represent the wave functions at the sites of the nonlinear trimer lattice, while the resonant frequencies of the circuit lattice correspond to the energy spectra.

In the linear regime, which is realized when $\psi_n^{A,B,C}$ approaches 0, the trimer circuit lattice exhibits three dispersive bands with two band gaps under periodic bound-

ary condition (see Supplementary Note 2 for the discussion of the linear trimer circuit lattice). Since the linear trimer lattice is inversion symmetric, i.e., $PH(k)P^{-1} = H(-k)$ with the inversion operator P and Hamiltonian in reciprocal space $H(k)$, the Zak phase defined as $\mathcal{Z} = i \int_{\text{BZ}} \langle \psi_k | \partial_k | \psi_k \rangle dk$ is quantized and can take only the values zero or π (modulo 2π). When the intracell hopping J is smaller than the intercell hopping J' , the linear trimer lattice is topologically nontrivial with $\mathcal{Z} = \pi$, 0, and π for the bottom, middle, and top bands, respectively. According to the bulk-boundary correspondence, one pair of edge states appear in each topological bandgap [53–57]. The edge states in the bottom gap feature two antisymmetric peaks at the two outermost sites, while the states in the top gap exhibit symmetric internal structures.

In the nonlinear regime, the theoretically calculated voltage-dependent energy spectra are illustrated in Fig. 2a. The solid curves represent the edge solitons, and the shaded regions depict the energy spectrum of the linear bulk bands. We use the voltage at the first leftmost site ψ_1^A to characterize the strength of circuit nonlinearity. We focus solely on the edge solitons located at the left termination of the trimer circuit lattice. Under weak nonlinearity, as indicated by the two violet curves near $\psi_1^A \rightarrow 0$, the topological edge solitons bifurcate from the linear topological edge states. Inherited from the internal structures of the linear edge states, the topological edge solitons in the bottom topological gap exhibit the antisymmetric peaks at the two leftmost sites, while those in the top topological gap display symmetric voltage distributions [see profiles of states (1) and (2) in Fig. 2b]. As ψ_1^A increases, the topological edge solitons become delocalized upon entering the linear bulk bands (see Supplementary Note 3 for complete energy spectra) [30]. However, as indicated by the blue curves, new families of edge solitons emerge in the top topological gap and semi-infinite gap [see states (3)-(5) and their corresponding branches]. States (3) and (4) both exhibit the antisymmetric internal structures, but state (3) exists only within a narrow region of the top topological gap and becomes delocalized upon entering the linear bulk band. Although the branch for state (5) is close to that of the symmetric topological edge soliton [state (2)], it displays a strongly asymmetric profile at the two leftmost sites. When the nonlinearity becomes sufficiently strong, self-sustained states emerge at the edge of the trimer lattice, where nonlinearity dominates the couplings. States (6)-(8) in Fig. 2b show typical profiles of three types of edge solitons with antisymmetric, symmetric, and asymmetric internal structures, respectively. These edge solitons are nonlinearity-induced conventional edge solitons and they are nontopological [58]. Among all the edge solitons shown in Fig. 2b, states (6)-(8) exhibit the strongest localization with observable voltage distributions concentrated almost entirely at the two leftmost sites [or solely

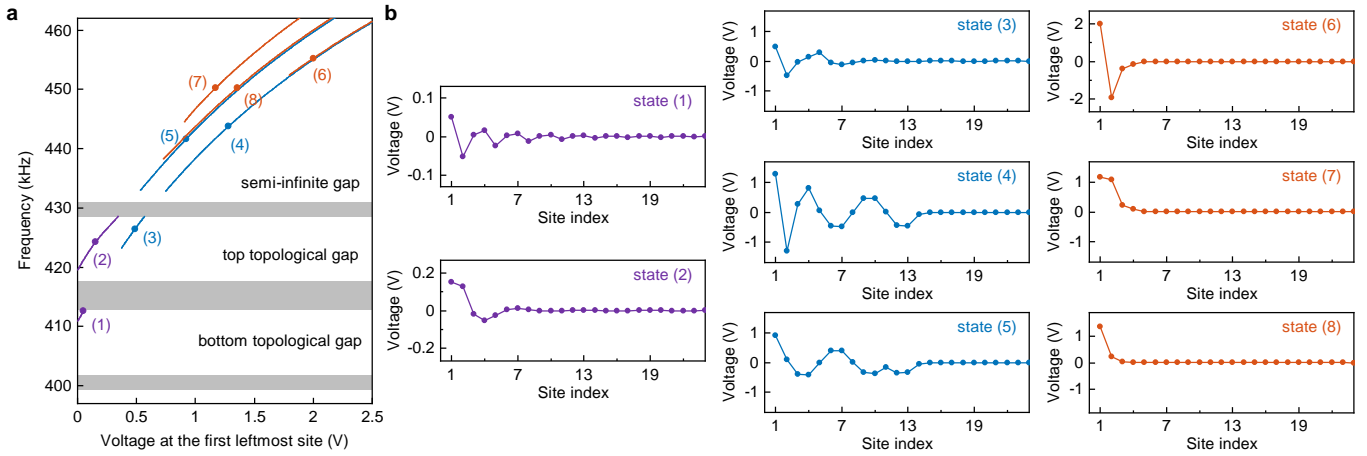


FIG. 2. **a**, Energy spectra as a function of the voltage at the first leftmost site ψ_1^A . The shaded regions are the bulk bands of the linear spectrum. **b**, Profiles of the edge solitons as indicated in (a).

at the first leftmost site for state (8)].

To experimentally investigate the topological and non-topological edge solitons and their phase transition, we implement quench dynamics in the nonlinear trimer circuit lattice. Following the principle shown in Fig. 1b, we initialize $\psi_n^{A,B}(t=0)$ to match the internal structures of the edge solitons. Specifically, for antisymmetric edge solitons, we set $V_{DC}^A = \psi_0$ and $V_{DC}^B = -\psi_0$; for symmetric edge solitons, both V_{DC}^A and V_{DC}^B equal ψ_0 ; and for asymmetric edge solitons, $V_{DC}^A = \psi_0$ and $V_{DC}^B = 0$. We then record the voltage distributions in the circuit lattice at various times. Similar to nonlinear waveguide arrays, where nonlinearity is dependent on optical power [30], the circuit nonlinearity here can be controlled by the value of ψ_0 .

In Figs. 3a-b, we present the experimentally measured and theoretically calculated temporal evolutions of the voltage envelopes under antisymmetric excitations. For $\psi_0 = 0.02$ V, i.e., under weak nonlinearity, the dynamic stability of the antisymmetric topological edge solitons (see Supplementary Note 3 for stability analysis) and the substantial overlap between the initial voltage distribution and state (1) in Fig. 2 enable the system to achieve a steady state before the voltages decay to undetectable levels. Consequently, we observe the formation of the antisymmetric topological edge soliton. Experimentally, the slight asymmetry between ψ_1^A and ψ_1^B is due to noise from the analog switches and unequal circuit dissipations at the two circuit nodes. For $\psi_0 = 2.5$ V (strong nonlinearity), we observe the formation of state (6) in Fig. 2, which represents the antisymmetric non-topological edge soliton with strong localization. This results from the nearly perfect overlap between the initial voltage distribution and soliton profiles, along with the approximate dynamic stability of these solitons across a broad voltage range. Under medium nonlinearities with $\psi_0 = 0.2, 0.5, 0.65$, and 1.2 V, the leftmost two sites still

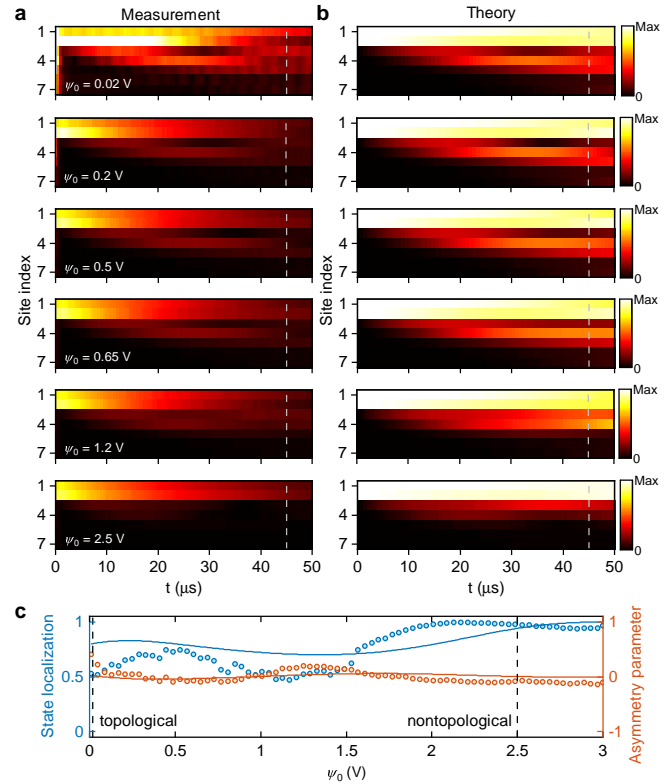


FIG. 3. **a-b**, Experimentally measured and theoretically calculated temporal evolutions under the antisymmetric excitations. **c**, State localizations and asymmetry parameters extracted from the voltage distributions at $t = 45 \mu\text{s}$ [indicated by the dashed lines in (a)-(b)]. The curves and scatter points denote the theoretical and experimental results, respectively.

exhibit the highest voltages. When the excitation voltage corresponds to a delocalized state or a strongly unstable edge soliton, the voltage localizes at these two sites due to the limited measurement time (See Supplementary Note

4). If the excitation voltage corresponds to a weakly unstable edge soliton, the initial voltage may excite the edge soliton, but the localized voltage will eventually collapse. In contrast, for a circuit lattice with $J > J'$, which is topologically trivial in the linear limit, voltage diffraction with local oscillations occurs throughout the entire range of excitation voltage, indicating the absence of edge solitons with antisymmetric internal structures (see Supplementary Note 5).

To quantitatively characterize the excitation of antisymmetric edge solitons during quench dynamics, we define the state localization S_2 as follows:

$$S_2 = \frac{|\psi_1^A|^2 + |\psi_1^B|^2}{\sum_n (|\psi_n^A|^2 + |\psi_n^B|^2 + |\psi_n^C|^2)}. \quad (4)$$

This measures the voltages of the two leftmost sites relative to the total voltage across all circuit nodes. Additionally, we introduce the asymmetry parameter Θ to quantify the imbalance between the voltages of these two sites:

$$\Theta = \frac{|\psi_1^A| - |\psi_1^B|}{|\psi_1^A| + |\psi_1^B|}. \quad (5)$$

We extract the voltage distributions at $t = 45 \mu\text{s}$, and the results for the state localization and asymmetry parameter are presented in Fig. 3c. State localization is relatively high when ψ_0 is near 0 or exceeds 2.5 V, as this leads to the formation of topological and nontopological edge solitons under weak and strong nonlinearities, respectively. Notably, the nontopological edge solitons [state (8) in Fig. 2] are generally more localized than the topological ones [state (2)], resulting in $P \approx 1$ for $\psi_0 > 2.5$ V. This indicates a phase transition from topological edge solitons under weak nonlinearity to nontopological ones under strong nonlinearity. Throughout this transition, the antisymmetric internal structure of the edge soliton is preserved, as the asymmetry parameter Θ remains approximately zero, as shown in Fig. 3c.

Similarly, we investigate the temporal evolutions of site voltages under symmetric excitations. As shown in Figs. 4a-b, the formation of the symmetric topological edge soliton [state (2) in Fig. 2] is observed under weak nonlinearity with $\psi_0 = 0.02$ V, again attributed to the dynamic stability of the topological edge soliton and significant overlap of the excitation (see Supplementary Note 3). Under medium nonlinearities, the leftmost two sites display the highest voltages due to the limited measurement time. For a longer evolution time, voltage diffraction or oscillation occurs as the excitation corresponds to a delocalized state or dynamically unstable edge soliton (see Supplementary Note 4). Even for $\psi_0 = 2$ V, in the regime of strong nonlinearity, the nontopological edge soliton [state (7) in Fig. 2] can only be discovered for a short duration before evolving into the asymmetric nontopological edge soliton [state (8)] due to instability.

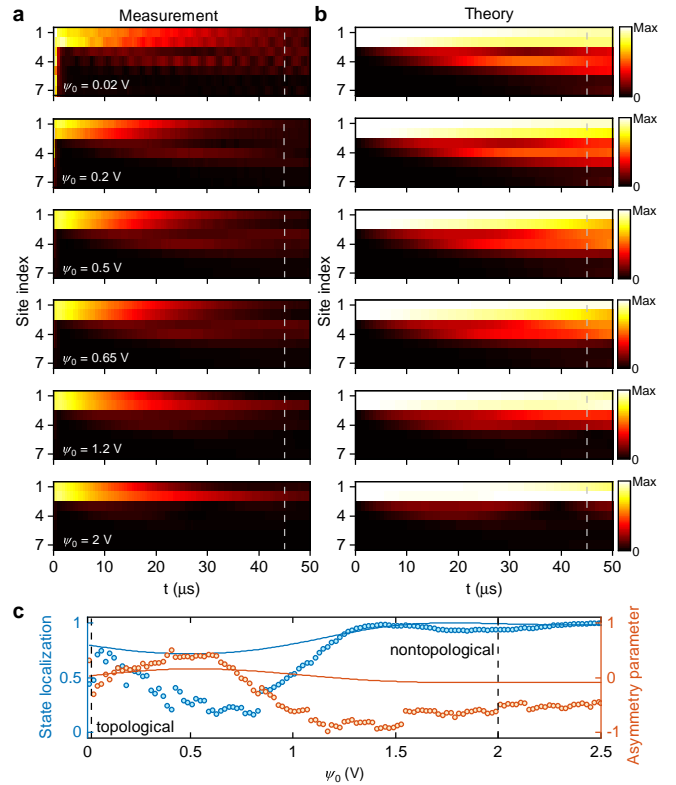


FIG. 4. **a-b**, The experimentally measured and theoretically calculated temporal evolutions under the symmetric excitations. **c**, The state localizations and asymmetry parameters extracted from the voltage distributions at $t = 45 \mu\text{s}$ [indicated by the dashed lines in (a)-(b)].

For a circuit lattice with $J > J'$, voltage diffraction is observed throughout the entire parameter range, indicating the absence of symmetric edge solitons (see Supplementary Note 5). In Fig. 4c, the enhanced state localization indicates a phase transition from topological edge solitons under weak nonlinearity to nontopological edge solitons under strong nonlinearity, and the nearly zero asymmetry parameters imply the preservation of the symmetric internal structure of the edge solitons.

To further clarify the differences in edge soliton types between the topological and nontopological phases, we study quench dynamics under the single-site excitations. From Figs. 5a-b, we observe voltage oscillations between the leftmost two sites under weak nonlinearity. These oscillations are induced by the overlap of the linear topological edge states with antisymmetric and symmetric internal structures (see Supplementary Note 4). Under medium nonlinearity, the asymmetric edge soliton [state (5) in Fig. 2] does not form due to its strong instability and weak localization (see Supplementary Note 3). However, when the nonlinearity is sufficiently strong, we observe the formation of the asymmetric nontopological edge soliton [state (8)]. This observation is further veri-

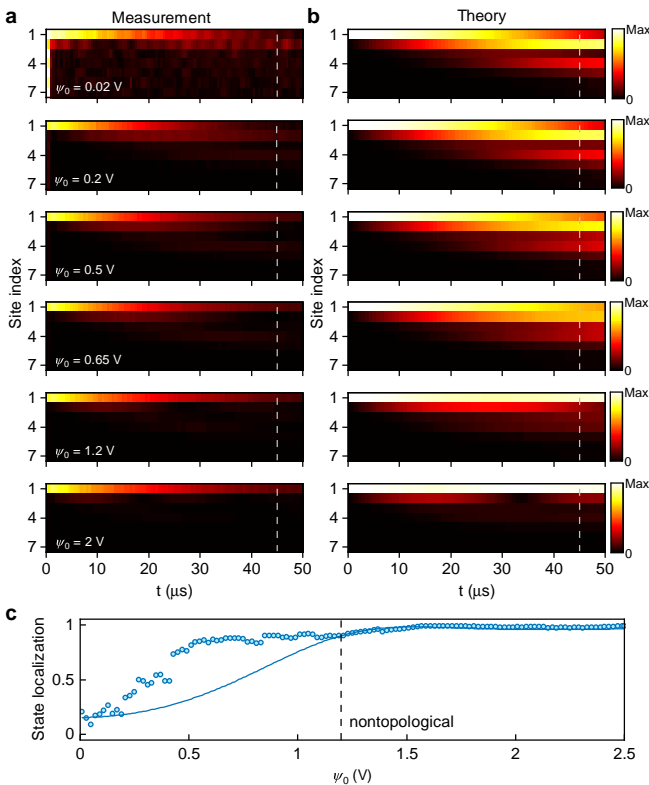


FIG. 5. **a-b**, The experimentally measured and theoretically calculated temporal evolutions under the single-site excitations. **c**, The state localizations extracted from the voltage distributions at $t = 45 \mu$ s.

fied by a modified definition of state localization:

$$S_1 = \frac{|\psi_1^A|^2}{\sum_n (|\psi_n^A|^2 + |\psi_n^B|^2 + |\psi_n^C|^2)}. \quad (6)$$

As shown in Fig. 5c, when ψ_0 is close to 0, state localization is low due to the voltage oscillation to the second site. In contrast, we find that P is approximately 1 when ψ_0 is greater than 1.2 V, indicating a significant enhancement in state localization. The above results indicate that there are no asymmetric topological edge solitons under weak nonlinearity, while asymmetric nontopological edge solitons do exist under strong nonlinearity. Additionally, asymmetric edge solitons do not exist in the topologically trivial lattice (see Supplementary Note 5).

In conclusion, we implement quench dynamics in a nonlinear trimer circuit lattice with tunable nonlinearity and observe the temporal evolutions of site voltages under the different initial excitations. We experimentally identify the antisymmetric and symmetric topological edge solitons under weak nonlinearity, as well as the nontopological edge solitons with antisymmetric, symmetric, and asymmetric internal structures under strong nonlinearity. Additionally, we confirm the phase transition between the topological and nontopological edge

solitons. Our findings pave the way for further exploration of nonlinear topological physics in circuit lattices and provide valuable insights into the interplay between topology and nonlinearity.

The authors thank fruitful discussions with Y. V. Kartashov and Y. Li. R.L., X.K., and W.W. was sponsored by the National Key Research and Development Program of China (Grant No. 2022YFA1404902) and National Natural Science Foundation of China (Grant No. 12104353). Y.L. was sponsored by the National Natural Science Foundation of China (NSFC) under Grant No. 62271366 and the 111 Project. The numerical calculations in this paper are supported by High-Performance Computing Platform of Xidian University.

* Corresponding author: rujiangli@xidian.edu.cn

† Corresponding author: coldfire2000@mail.xjtu.edu.cn

‡ Corresponding author: liuying@mail.xidian.edu.cn

- [1] M. Z. Hasan and C. L. Kane, Colloquium: Topological Insulators, *Rev. Mod. Phys.* 82, 3045 (2010).
- [2] X.-L. Qi and S.-C. Zhang, Topological Insulators and Superconductors, *Rev. Mod. Phys.* 83, 1057 (2011).
- [3] O. Breunig and Y. Ando, Opportunities in Topological Insulator Devices, *Nat. Rev. Phys.* 4, 184 (2022).
- [4] G. Ma, M. Xiao, and C. T. Chan, Topological Phases in Acoustic and Mechanical Systems, *Nat. Rev. Phys.* 1, 281 (2019).
- [5] H. Xue, Y. Yang, and B. Zhang, Topological Acoustics, *Nat. Rev. Mater.* 7, 974 (2022).
- [6] N. R. Cooper, J. Dalibard, and I. B. Spielman, Topological Bands for Ultracold Atoms, *Rev. Mod. Phys.* 91, 015005 (2019).
- [7] Z.-K. Lin, Q. Wang, Y. Liu, H. Xue, B. Zhang, Y. Chong, and J.-H. Jiang, Topological Phenomena at Defects in Acoustic, Photonic and Solid-State Lattices, *Nat. Rev. Phys.* 5, 483 (2023).
- [8] B. Xie, H.-X. Wang, X. Zhang, P. Zhan, J.-H. Jiang, M. Lu, and Y. Chen, Higher-Order Band Topology, *Nat. Rev. Phys.* 3, 520 (2021).
- [9] T. Shah, C. Brendel, V. Peano, and F. Marquardt, Colloquium: Topologically Protected Transport in Engineered Mechanical Systems, *Rev. Mod. Phys.* 96, 021002 (2024).
- [10] T. Ozawa et al., Topological Photonics, *Rev. Mod. Phys.* 91, 015006 (2019).
- [11] M. Kim, Z. Jacob, and J. Rho, Recent Advances in 2D, 3D and Higher-Order Topological Photonics, *Light: Science & Applications* 9, 1 (2020).
- [12] D. Smirnova, D. Leykam, Y. Chong, and Y. Kivshar, Nonlinear Topological Photonics, *Applied Physics Reviews* 7, 021306 (2020).
- [13] A. Szameit and M. C. Rechtsman, Discrete Nonlinear Topological Photonics, *Nat. Phys.* 20, 905 (2024).
- [14] M. J. Ablowitz, C. W. Curtis, and Y.-P. Ma, Linear and Nonlinear Traveling Edge Waves in Optical Honeycomb Lattices, *Phys. Rev. A* 90, 023813 (2014).
- [15] D. Leykam and Y. D. Chong, Edge Solitons in Nonlinear-Photonic Topological Insulators, *Phys. Rev. Lett.* 117, 143901 (2016).

- [16] Y. Lumer, M. C. Rechtsman, Y. Plotnik, and M. Segev, Instability of Bosonic Topological Edge States in the Presence of Interactions, *Phys. Rev. A* 94, 021801 (2016).
- [17] Y. V. Kartashov and D. V. Skryabin, Modulational Instability and Solitary Waves in Polariton Topological Insulators, *Optica* 3, 1228 (2016).
- [18] Y. V. Kartashov and D. V. Skryabin, Bistable Topological Insulator with Exciton-Polaritons, *Phys. Rev. Lett.* 119, 253904 (2017).
- [19] D. A. Dobrykh, A. V. Yulin, A. P. Slobozhanyuk, A. N. Poddubny, and Yu. S. Kivshar, Nonlinear Control of Electromagnetic Topological Edge States, *Phys. Rev. Lett.* 121, 163901 (2018).
- [20] W. Zhang, X. Chen, Y. V. Kartashov, V. V. Konotop, and F. Ye, Coupling of Edge States and Topological Bragg Solitons, *Phys. Rev. Lett.* 123, 254103 (2019).
- [21] D. A. Smirnova, L. A. Smirnov, D. Leykam, and Y. S. Kivshar, Topological Edge States and Gap Solitons in the Nonlinear Dirac Model, *Laser & Photonics Reviews* 13, 1900223 (2019).
- [22] Y.-L. Tao, N. Dai, Y.-B. Yang, Q.-B. Zeng, and Y. Xu, Hinge Solitons in Three-Dimensional Second-Order Topological Insulators, *New J. Phys.* 22, 103058 (2020).
- [23] M. Guo, S. Xia, N. Wang, D. Song, Z. Chen, and J. Yang, Weakly Nonlinear Topological Gap Solitons in Su-Schrieffer-Heeger Photonic Lattices, *Opt. Lett.* 45, 6466 (2020).
- [24] Z. Zhang et al., Observation of Edge Solitons in Photonic Graphene, *Nat. Commun.* 11, 1902 (2020).
- [25] S. Mukherjee and M. C. Rechtsman, Observation of Unidirectional Solitonlike Edge States in Nonlinear Floquet Topological Insulators, *Phys. Rev. X* 11, 041057 (2021).
- [26] T. Tuloup, Nonlinearity Induced Topological Physics in Momentum Space and Real Space, *Phys. Rev. B* 102, 115411 (2020).
- [27] M. S. Kirsch, Y. Zhang, M. Kremer, L. J. Maczewsky, S. K. Ivanov, Y. V. Kartashov, L. Torner, D. Bauer, A. Szameit, and M. Heinrich, Nonlinear Second-Order Photonic Topological Insulators, *Nat. Phys.* 17, 995 (2021).
- [28] N. Pernet et al., Gap Solitons in a One-Dimensional Driven-Dissipative Topological Lattice, *Nat. Phys.* 18, 678 (2022).
- [29] M. Ezawa, Nonlinearity-Induced Chiral Solitonlike Edge States in Chern Systems, *Phys. Rev. B* 106, 195423 (2022).
- [30] Y. V. Kartashov et al., Observation of Edge Solitons in Topological Trimer Arrays, *Phys. Rev. Lett.* 128, 093901 (2022).
- [31] M. Ezawa, Nonlinearity-Induced Transition in the Nonlinear Su-Schrieffer-Heeger Model and a Nonlinear Higher-Order Topological System, *Phys. Rev. B* 104, 235420 (2021).
- [32] L. Lu, Topology on a Breadboard, *Nature Phys.* 14, 875 (2018).
- [33] C. H. Lee, S. Imhof, C. Berger, F. Bayer, J. Brehm, L. W. Molenkamp, T. Kiessling, and R. Thomale, Topoelectrical Circuits, *Commun. Phys.* 1, 39 (2018).
- [34] E. Zhao, Topological Circuits of Inductors and Capacitors, *Annals of Physics* 399, 289 (2018).
- [35] J. Dong, V. Juričić, and B. Roy, Topoelectric Circuits: Theory and Construction, *Phys. Rev. Research* 3, 023056 (2021).
- [36] H. Yang, L. Song, Y. Cao, and P. Yan, Circuit realization of topological physics, *Physics Reports* 1093, 1 (2024).
- [37] X. Zheng, T. Chen, W. Zhang, H. Sun, and X. Zhang, Exploring Topological Phase Transition and Weyl Physics in Five Dimensions with Electric Circuits, *Phys. Rev. Research* 4, 033203 (2022).
- [38] Y. Wang, H. M. Price, B. Zhang, and Y. D. Chong, Circuit Implementation of a Four-Dimensional Topological Insulator, *Nat. Commun.* 11, 2356 (2020).
- [39] S. Imhof et al., Topoelectrical-Circuit Realization of Topological Corner Modes, *Nature Phys* 14, 925 (2018).
- [40] S. Liu, S. Ma, Q. Zhang, L. Zhang, C. Yang, O. You, W. Gao, Y. Xiang, T. J. Cui, and S. Zhang, Octupole Corner State in a Three-Dimensional Topological Circuit, *Light: Science & Applications* 9, 145 (2020).
- [41] T. Helbig, T. Hofmann, S. Imhof, M. Abdelghany, T. Kiessling, L. W. Molenkamp, C. H. Lee, A. Szameit, M. Greiter, and R. Thomale, Generalized Bulk-boundary Correspondence in Non-Hermitian Topoelectrical Circuits, *Nat. Phys.* 16, 747 (2020).
- [42] S. Liu, R. Shao, S. Ma, L. Zhang, O. You, H. Wu, Y. J. Xiang, T. J. Cui, and S. Zhang, Non-Hermitian Skin Effect in a Non-Hermitian Electrical Circuit, *Research* 2021, 5608038 (2021).
- [43] D. Zou, T. Chen, W. He, J. Bao, C. H. Lee, H. Sun, and X. Zhang, Observation of Hybrid Higher-Order Skin-Topological Effect in Non-Hermitian Topoelectrical Circuits, *Nat. Commun.* 12, 7201 (2021).
- [44] J. Wu et al., Non-Abelian Gauge Fields in Circuit Systems, *Nat. Electron.* 5, 635 (2022).
- [45] Q. Guo, T. Jiang, R.-Y. Zhang, L. Zhang, Z.-Q. Zhang, B. Yang, S. Zhang, and C. T. Chan, Experimental Observation of Non-Abelian Topological Charges and Edge States, *Nature* 594, 195 (2021).
- [46] W. Zhang, H. Yuan, N. Sun, H. Sun, and X. Zhang, Observation of Novel Topological States in Hyperbolic Lattices, *Nat. Commun.* 13, 2937 (2022).
- [47] W. Zhang, F. Di, X. Zheng, H. Sun, and X. Zhang, Hyperbolic Band Topology with Non-Trivial Second Chern Numbers, *Nat. Commun.* 14, 1083 (2023).
- [48] Y. Hadad, J. C. Soric, A. B. Khanikaev, and A. Alù, Self-Induced Topological Protection in Nonlinear Circuit Arrays, *Nat Electron* 1, 178 (2018).
- [49] Y. Wang, L.-J. Lang, C. H. Lee, B. Zhang, and Y. D. Chong, Topologically Enhanced Harmonic Generation in a Nonlinear Transmission Line Metamaterial, *Nat Commun* 10, 1102 (2019).
- [50] F. Zangeneh-Nejad and R. Fleury, Nonlinear Second-Order Topological Insulators, *Phys. Rev. Lett.* 123, 053902 (2019).
- [51] T. Kotwal, F. Moseley, A. Stegmaier, S. Imhof, H. Brand, T. Kießling, R. Thomale, H. Ronellenfitsch, and J. Dunkel, Active Topoelectrical Circuits, *Proc. Natl. Acad. Sci. U.S.A.* 118, e2106411118 (2021).
- [52] H. Hohmann et al., Observation of Cnoidal Wave Localization in Nonlinear Topoelectric Circuits, *Phys. Rev. Research* 5, L012041 (2023).
- [53] L. Jin, Topological Phases and Edge States in a Non-Hermitian Trimerized Optical Lattice, *Phys. Rev. A* 96, 032103 (2017).
- [54] V. M. Martinez Alvarez and M. D. Coutinho-Filho, Edge States in Trimer Lattices, *Phys. Rev. A* 99, 013833 (2019).
- [55] R. Li and Y. Hadad, Reduced Sensitivity to Disorder in a Coupled-Resonator Waveguide with Disordered Coupling Coefficients, *Phys. Rev. A* 103, 023503 (2021).

- [56] Y. Wang, Y.-H. Lu, J. Gao, Y.-J. Chang, H. Tang, and X.-M. Jin, Experimental Topological Photonic Superlattice, *Phys. Rev. B* 103, 014110 (2021).
- [57] A. Anastasiadis, G. Styliaris, R. Chaunsali, G. Theocharis, and F. K. Diakonov, Bulk-Edge Correspondence in the Trimer Su-Schrieffer-Heeger Model, *Phys. Rev. B* 106, 085109 (2022).
- [58] F. Lederer, G. I. Stegeman, D. N. Christodoulides, G. Assanto, M. Segev, and Y. Silberberg, Discrete Solitons in Optics, *Physics Reports* 463, 1 (2008).